INTERNATIONAL JOURNAL FOR NUMERICAL AND ANALYTICAL METHODS IN GEOMECHANICS
Int. J. Numer. Anal. Meth. Geomech., 2007; **31**:1257–1279
Published online 3 January 2007 in Wiley InterScience (www.interscience.wiley.com). DOI: 10.1002/nag.579

A density-dependent elastoplastic hydro-mechanical model for unsaturated compacted soils

D. A. Sun[1,*,†], D. C. Sheng[2], H. B. Cui[3] and S. W. Sloan[2]

[1] *Department of Civil Engineering, Shanghai University, 149 Yanchang Road, Shanghai 200072, China*
[2] *School of Engineering, University of Newcastle, NSW 2308, Australia*
[3] *Department of Civil Engineering, Nagoya Institute of Technology, Nagoya 466-8555, Japan*

SUMMARY

This paper presents a three-dimensional elastoplastic constitutive model for predicting the hydraulic and mechanical behaviour of unsaturated soils. It is based on experimental results obtained from a series of controlled-suction triaxial tests on unsaturated compacted clay with different initial densities. Hydraulic hysteresis in the water-retention behaviour is modelled as an elastoplastic process, with the elastic part modelled by a series of scanning curves and the elastoplastic part modelled by the main drying and wetting curves. The effect of void ratio on the water-retention behaviour is studied using data obtained from controlled-suction wetting–drying cyclic tests on unsaturated compacted clay with different initial densities. The effect of the degree of saturation on the stress–strain-strength behaviour and the effect of void ratio on the water-retention behaviour are considered in the model, as is the effect of suction on the hydraulic and mechanical behaviour. The initial density dependency of the compacted soil behaviour is modelled by experimental relationships between the initial density and the corresponding yield stress and, thereby, between the initial density and the normal compression line. The model is generalized to three-dimensional stress states by assuming that the shapes of the failure and yield surfaces in the deviatoric stress plane are given by the Matsuoka–Nakai criterion. Model predictions of the stress–strain and water-retention behaviour are compared with those obtained from triaxial tests with different initial densities under isotropic compression, triaxial compression and triaxial extension, with or without variation in suction. The comparisons indicate that the model accurately predicts the hydraulic and mechanical behaviour of unsaturated compacted soils with different initial densities using the same material constant.

Received 27 September 2005; Revised 19 August 2006; Accepted 14 October 2006

KEY WORDS: unsaturated soil; elastoplastic; constitutive equation; suction; water-retention curve; triaxial test

*Correspondence to: D. A. Sun, Department of Civil Engineering, Shanghai University, 149 Yanchang Road, Shanghai 200072, China.
† E-mail: sundean06@163.com

Contract/grant sponsor: Australian Research Council; contract/grant number: DP0344417
Contract/grant sponsor: National Natural Science Foundation of China; contract/grant number: 10572082

1. INTRODUCTION

Since the pioneering work of Alonso *et al.* [1], several elastoplastic constitutive models for unsaturated soils have been proposed (e.g. [2–4]). The stress-state variables employed in early models are the net stress (the difference between the total stress and pore-air pressure) and the suction (the difference between the pore-air pressure and pore-water pressure), while the strain-state variables are the soil skeleton strains. In these models, the influence of unsaturation is expressed only in terms of the suction. The degree of saturation is computed from the suction separately using the so-called soil–water-characteristic curve (SWCC), and thus hydraulic hysteresis is not directly incorporated into the constitutive model. In recent years, some conceptual models incorporating hydraulic hysteresis of unsaturated soils have been proposed [5–10]. However, most of these models can only describe the hydraulic and stress–strain behaviour in qualitative terms or are only formulated for isotropic stress conditions. To avoid this shortcoming, Sun and Sheng [11] have proposed a complete formulation of an elastoplastic constitutive model which incorporates the hydraulic and mechanical behaviour of unsaturated soils, and quantitatively compared its predictions with experimental results obtained from controlled-suction isotropic compression tests and triaxial compression tests on unsaturated compacted soil. This model, however, is only applicable to unsaturated soil with one initial density. Since the initial density of unsaturated compacted soil varies with the compaction energy, this means that the same soil with different initial densities has to be modelled as different materials. Sun *et al.* [12] have proposed an elastoplastic constitutive model for predicting the mechanical behaviour of unsaturated compacted soils with different initial densities. The model predictions are in good agreement with experimental results obtained by the first author and also with those published more recently by Estabragh *et al.* [13]. However, the model can only predict the mechanical behaviour of unsaturated compacted soil with the degree of saturation not being considered. In this paper we develop an elastoplastic constitutive model which is capable of predicting the hydraulic and mechanical behaviour of unsaturated soils that are compacted at different initial densities.

The paper is organized as follows. First, we describe controlled-suction isotropic compression tests on unsaturated clay, compacted at different initial densities, which were conducted along various wetting paths, drying paths, and compression paths with measurement of the degree of saturation. Secondly, a three-dimensional elastoplastic model for unsaturated soils with different initial densities, which incorporates both the mechanical and hydraulic behaviour, is formulated. Finally, the model predictions are compared with the experimental results obtained from isotropic compression tests, triaxial compression tests, and triaxial extension tests on unsaturated compacted clay with different initial densities.

2. DENSITY EFFECTS

In order to investigate the influence of void ratio on the water-retention and mechanical behaviour, a series of isotropic compression tests on unsaturated compacted clay were performed using a suction-controllable triaxial apparatus. The soil used in this study is called Pearl clay. It contains 50% silt and 50% clay, and there is almost no expansive mineral content. Its liquid limit is 49% and its plasticity index is 22%. Triaxial specimens were prepared by compaction in a mold at a water content of about 26%. Specimens were compacted in five

DOI: 10.1002/nag

layers, with each layer statically compacted 15 times up to a specific vertical stress using a 1.2 cm diameter plunger, and are on the dry side of optimum [14]. The initial void ratio and initial degree of saturation were controlled by changing the compaction energy.

The triaxial apparatus used can directly measure the radial strain of the specimens, and can also control the matric suction. The radial displacement of the specimen was measured using three stainless steel rings mounted at $H/4$, $H/2$ and H from the top of the specimen, with H being the specimen height [12, 14]. The average radial strain was calculated based on the assumption that the lateral shape of the deformed specimen can be approximated by a third-order polynomial. The specimen height was 8 cm for measuring the stress–strain relations and 3.5 cm for measuring the water-retention behaviour, while the diameter of the specimens was about 3.5 cm. The pore-water pressure was maintained at atmospheric pressure during the constant suction tests, drying tests and wetting tests through a ceramic disk installed in the pedestal with an air-entry value of 300 or 500 kPa. The pore-air pressure was applied at the top through a one way filter that prevented water from seeping out. Hence, the change in the water volume in the burette is the same as the change in the water volume of the test specimen, thus allowing the degree of saturation to be calculated. For further details, see [4, 12, 14]. The imposed stress paths in each case were varied, depending on the objective of each test. The detailed stress path of each particular test will be explained when the results are described.

Figure 1 shows the water-retention curves for an unsaturated specimen compacted at initial void ratios of $e_0 = 1.08$ and 1.78. Figure 1(a) was obtained by decreasing the matric suction from 196 to about 2 kPa (segment AB), increasing the suction from about 2 to 490 kPa (segment BC), and then decreasing the suction from 490 to about 2 kPa (segment CD) under a constant isotropic net stress of 20 kPa. The specimen was first isotropically consolidated at a mean total

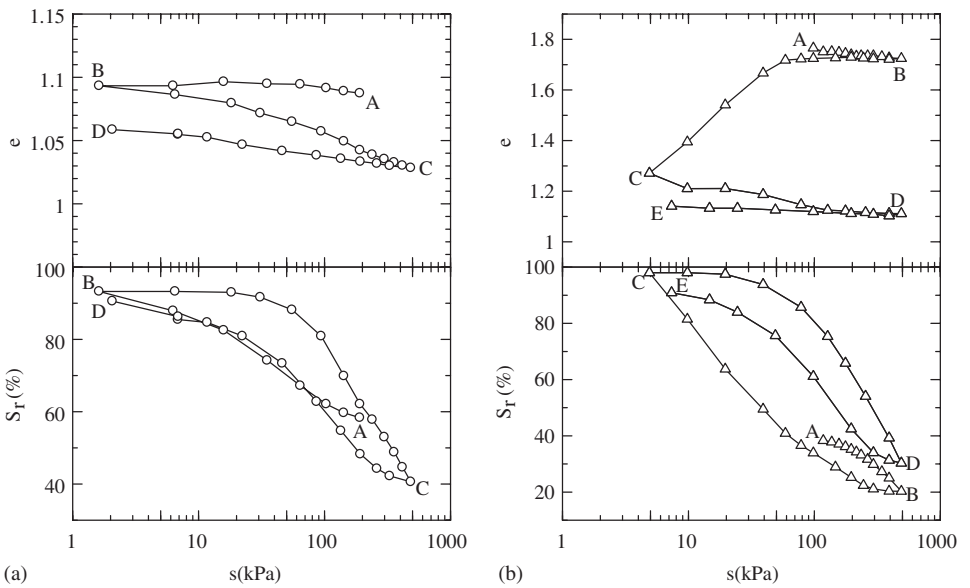

Figure 1. Wetting–drying cycles performed on Pearl clay specimen compacted at different void ratios under isotropic net stress of 20 kPa. (a) $e_0 = 1.08$; and (b) $e_0 = 1.78$.

DOI: 10.1002/nag

stress $\bar{p}$ of 20 kPa with an initial suction, and then an air pressure u_a of 196 kPa was applied to the specimens with a mean net stress p of 20 kPa (where the mean net stress $p = \bar{p} - u_a$). The drainage valve was then opened to dissipate the pore-water pressure so that $u_w = 0$. Figure 1(a) shows the changes in the void ratio and the degree of saturation during the wetting, drying and re-wetting paths under $p = 20$ kPa. Because the specimen was densely compacted there is no noticeable compression or swelling as the suction is decreased along path AB. However, a little swelling was observed when the suction was decreased along the path CD. This may be because the specimen becomes denser after the drying test in which some compression occurred during the suction increase (SI) process BC. The deformation behaviour is similar to the test results of a compacted kaolin reported by Wheeler *et al.* [9].

The wetting and drying branches form extreme bounds called the main wetting and drying curves. The segments between the main curves are the scanning curves. It can be seen from Figure 1(a) that the slope of the scanning curve is much less than those of the main curves and the second main wetting curve CD is almost the same as the first main wetting curve AB.

Figure 1(b) shows the water-retention curve of an unsaturated specimen compacted at an initial void ratio of 1.78, obtained by changing the suction under a constant isotropic net stress of 20 kPa. The specimens was first isotropically consolidated at a mean total stress $\bar{p}$ of 20 kPa, and then an air pressure of 98 kPa was applied to the specimens with the drainage valve being opened so that the pore-water pressure $u_w = 0$. After that the specimen was dried by increasing the imposed suction from 98 to 490 kPa (AB), wetted by decreasing the suction from 490 to 5 kPa (BC), dried by increasing the suction from 5 to 490 kPa (CD), and finally wetted by decreasing the suction from 490 to 7 kPa (DE). It can be seen that a large amount of compression occurs during the first wetting process (BC). After this collapse occurs there is no significant deformation during the drying process (CD) and wetting process (DE). As shown in Figure 1(b), the second cycle of the main wetting and drying curves are shifted to the right after collapse takes place. This is because the decrease in void ratio results in a decrease in connecting passageways between the voids, and hence an increase in the air-entry value [15]. Comparing Figure 1(a) with (b), we also can confirm the above conclusion, i.e. the denser the specimen the higher the degree of saturation at the same imposed suction and the main wetting and drying curves are dependent on the current density. Therefore, the water-retention curve of a compacted specimen is clearly density dependent. That is to say, the degree of saturation is not only dependent on the suction and its history but also dependent on the density.

Figure 2 shows the test results for Pearl clay under a constant suction [11]. The specimens are prepared using the same procedure as described previously. It can be seen that the relationship between the measured degree of saturation and the void ratio, for specimens with different initial void ratios, can be approximated by a straight line. Taking the above experimental results into account, the scanning curve, the main drying curve and the main wetting curve can be idealized by the relations [11]

$$S_r = S_{rs}^0 - \lambda_{se}(e - 1) - \kappa_s \ln \frac{s}{p_a} \tag{1}$$

$$S_r = S_{rD}^0 - \lambda_{se}(e - 1) - \lambda_D \ln \frac{s}{p_a} \tag{2}$$

$$S_r = S_{rW}^0 - \lambda_{se}(e - 1) - \lambda_W \ln \frac{s}{p_a} \tag{3}$$

DOI: 10.1002/nag

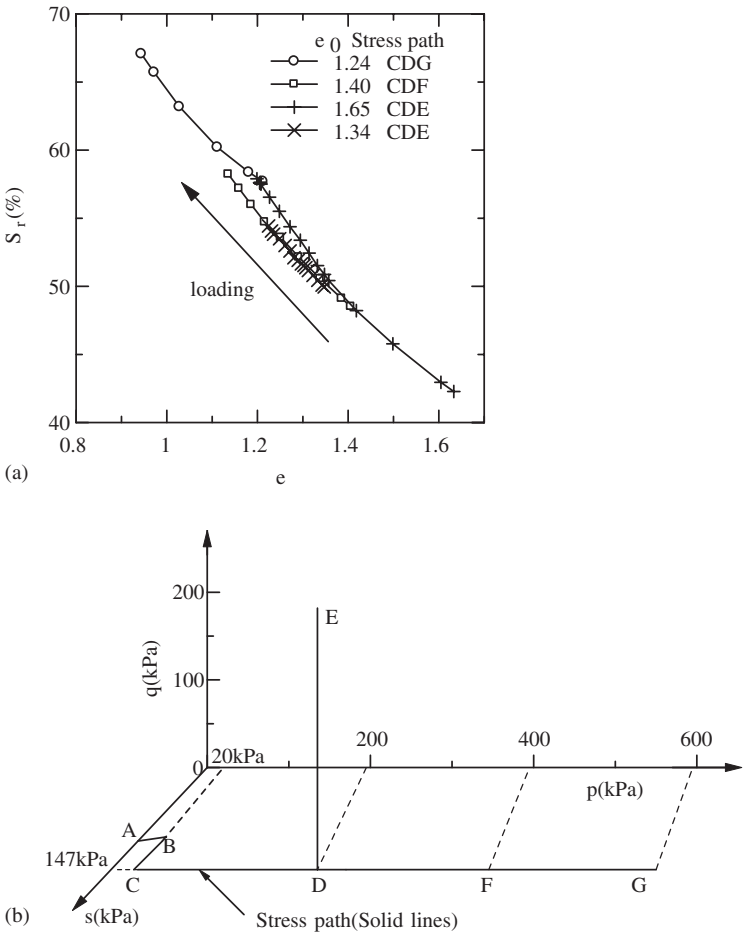

Figure 2. Relation between void ratio and degree of saturation during isotropic compression and triaxial shear tests under $s = 147$ kPa: (a) relation between viod ratio and degree of saturation; and (b) stress paths.

where s is the suction, S_{rs}^0, S_{rD}^0 and S_{rW}^0 are the degrees of saturation of the scanning curve and the main drying and wetting curves at $s = p_a$ (atmosphere pressure) and $e_0 = 1$, λ_{se} is the gradient of the S_r *versus* e relation under a constant suction, and κ_s, λ_D, and λ_w are the slopes of the scanning curve, the main drying curve and the main wetting curve on a plot of S_r against $\ln s$. Differentiating Equations (1)–(3) gives

$$dS_r = -\lambda_{se}\, de - \kappa_s \frac{ds}{s} \tag{4}$$

$$dS_r = -\lambda_{se}\, de - \lambda_D \frac{ds}{s} \tag{5}$$

$$dS_r = -\lambda_{se}\, de - \lambda_W \frac{ds}{s} \tag{6}$$

DOI: 10.1002/nag

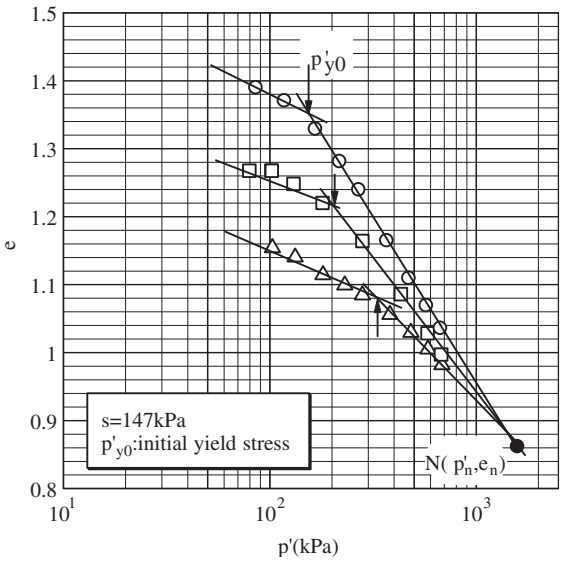

Figure 3. Results of isotropic compression tests on unsaturated clay compacted at different initial void ratios.

Figure 3 shows the results of isotropic compression tests on compacted specimens at different initial void ratios under $s = 147$ kPa. These specimens were prepared by statically compacting samples to different vertical stresses at the same water content of 26%. In Figure 3 and the following, $p' = p + S_r s$, where p' is called the mean 'effective stress'. It can be seen that even under the same imposed suction the yield stress increases as the initial void ratio of the compacted specimen decreases. The stiffness parameter $\lambda(s, e_c) = -\Delta e/\Delta \ln p'$, defined in the post-yield range for $s = 147$ kPa, decreases when the initial void ratio decreases. The plots in Figure 4 show the measured initial yield stresses p'_{y0} for compacted specimens at different initial void ratios under a suction of 147 kPa. Figure 4(a) shows the relationship between the initial void ratios of the compacted specimens and their corresponding initial yield stresses. The same results are also plotted as a relation between p'_{y0} and the corresponding void ratio e_c (i.e. the void ratio at $p' = p'_{y0}$) in Figure 4(b). The relationship between $\log p'_{y0}$ and $\log e_c$ can be approximated by the straight lines in Figure 4(b) and may be expressed as

$$p'_{y0}(s) = be_c(s)^c \tag{7}$$

where b and c are initial yield stress parameters at a reference suction s, with b being a model parameter and c being determined later.

3. AN ELASTOPLASTIC MODEL

3.1. Stress-state and strain-state variables for unsaturated soil

To identify the hydraulic and mechanical behaviour of unsaturated soils properly, the stress-state variables employed in the model are the 'effective stress' tensor σ'_{ij} and the suction s. The

DOI: 10.1002/nag

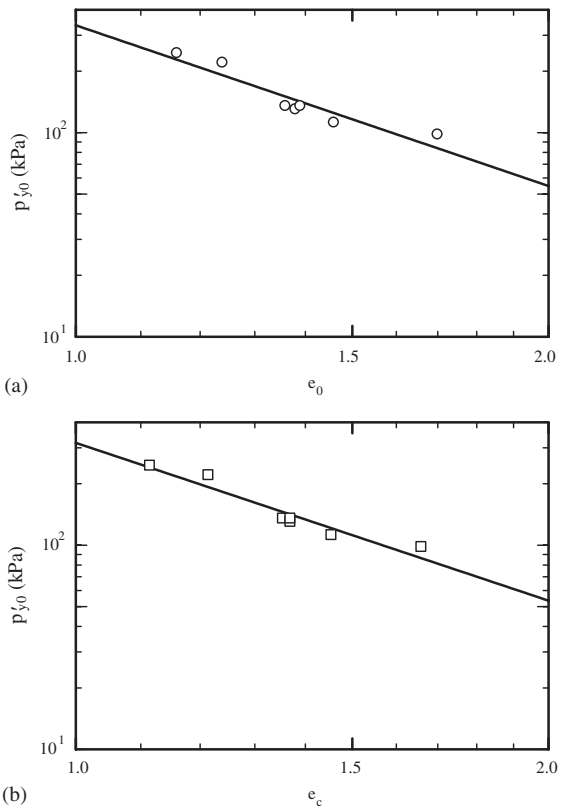

Figure 4. Measured initial yield stresses for specimens with different initial densities under suction of 147 kPa: (a) initial void ratio *versus* initial yield stress relationship; and (b) initial yield stress *versus* corresponding void ratio relationship.

'effective stress' tensor σ'_{ij} is defined as

$$\sigma'_{ij} = \bar{\sigma}_{ij} - u_a\delta_{ij} + S_r s\delta_{ij} = \sigma_{ij} + S_r s\delta_{ij} \tag{8}$$

where σ_{ij} is the net stress tensor, $\bar{\sigma}_{ij}$ is the total stress tensor, S_r is the saturation degree, u_a is the pore-air pressure and δ_{ij} is the Kronecker delta. Equation (8) is similar to the effective stress proposed by Bishop and Blight [16], with S_r taking the place of the weighting factor χ. The 'effective stress' automatically becomes Terzaghi's effective stress for the saturated state, and is the same as the 'average stress' [17], 'Bishop's stress' [9], and the 'constitutive stress' [10]. The first to use the degree of saturation, instead of the fractional contact area, as the weighting factor in the stress tensor appears to be Schrefler [18], who derived the stress tensor for three phase flow (water, gas and oil) in a porous medium and for partially saturated soil under static air pressure. Using S_r instead of χ leads to an effective stress definition that is independent of the material properties, since S_r is now treated as an independent variable just like $\bar{\sigma}_{ij}$ and s.

The strain-variables employed in the model are the soil skeleton strain and degree of saturation. As indicated by Houlsby [19], the stresses that are work-conjugate to the soil

DOI: 10.1002/nag

skeleton strain and the degree of saturation are the 'effective stress' and the modified suction $s' = ns$ (where n is the porosity). Here the suction s is chosen as one of the stress variables for the sake of experimental simplicity. The 'effective stress' and the suction are not independent variables, unlike their work-conjugate strains (the soil skeleton strains and the degree of saturation [10]). The stress-state and strain-state variables adopted in the present study permit a general form of hydraulic behaviour to be represented and also provide a smooth transition between the saturated and unsaturated states.

3.2. Formulation of the elastoplastic model for isotropic stress states

Following previous work [11, 12], a new model can be formulated which uses the 'effective stress' and suction as the stress-state variables instead of the translated stress and suction. A similar form is adopted in the stress–strain relation, except that the 'effective stress' is now defined as per Equation (8). Note that the translated stress is a combination of net stress and suction [4, 12], and does not account for the contribution of the degree of saturation to the 'effective stress' explicitly.

All the normal compression lines for unsaturated soil with different suctions and initial densities can be written as

$$e = e_{\mathrm{n}} - \lambda(s, e_{\mathrm{c}}) \ln \frac{p'_{\mathrm{y}}}{p'_{\mathrm{n}}} \tag{9}$$

where e_{n} and p'_{n} are material parameters [12], p'_{y} is the isotropic yield stress, and $\lambda(s, e_{\mathrm{c}})$ is the slope of the normal compression line of an unsaturated soil with suction s defined by

$$\lambda(s, e_{\mathrm{c}}) = \frac{e_{\mathrm{c}}(s) - e_{\mathrm{n}}}{\ln p'_{\mathrm{n}}/p'_{\mathrm{y0}}(s)} \tag{10}$$

The meanings of $p'_{\mathrm{y0}}(s)$ and $e_{\mathrm{c}}(s)$ can be found in Figure 5, which shows the initial yield stress curve CBN, a normal compression line BN for unsaturated soil with initial void ratio e_0 and suction s and the normal compression line DN for saturated soil. The curve CBN is expressed by Equation (7), while the slope of the line BN is $\lambda(s, e_{\mathrm{c}})$. When the initial state A (p_0, s, e_0) is given,

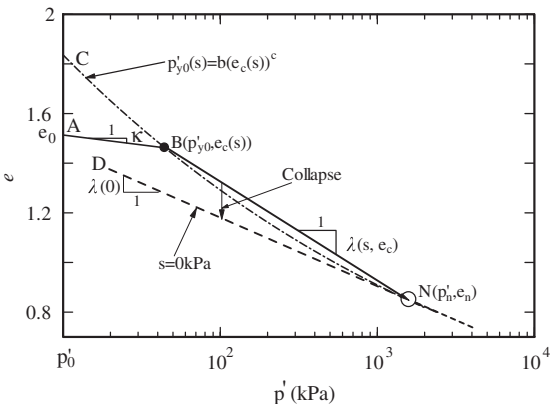

Figure 5. Initial density dependency of initial yield stress and normal compression line.

DOI: 10.1002/nag

the sample is assumed to move along AB and then BN under isotropic loading. The slope of AB is a material parameter κ, and the initial yield stress curve CBN is determinate for a given soil. Hence, point B can be calculated by solving Equation (7) and $e_c(s) = e_0 - \kappa \ln(p'_{y0}(s)/p'_0)$ simultaneously, where p'_0 is an initial stress for $e = e_0$ and $\lambda(s, e_c)$ is calculated using Equation (10). For any suction, the quantity $\lambda(s, e_c)$ is assumed as per Sun and Sheng [11]

$$\lambda(s, e_c) = \lambda(0) + \frac{\lambda(e_0)s}{s + p_a} \tag{11}$$

where $\lambda(0)$ is the slope of the normal compression line for saturated soils, $\lambda(e_0)$ is a parameter dependent on e_0, and p_a is atmospheric pressure.

Equation (10) gives the slopes of the normal compression lines for unsaturated soils with different initial void ratios but under a given suction s, while Equation (11) varies the slopes $\lambda(s, e_c)$ with suction s for a given initial void ratio. The method for determining $\lambda(s, e_c)$ for any suction and initial density is as follows. When the model parameters κ, b, c and initial state values e_0, p'_0 are given, $p'_{y0}(s_0)$ and $e_c(s_0)$ can be solved from Equation (7) and $e_c(s) = e_0 - \kappa \ln(p'_{y0}(s)/p'_0)$ for a given suction s_0. Substituting the values of $e_c(s_0)$ and $p'_{y0}(s_0)$ into Equation (10) gives $\lambda(s_0, e_c)$, and then substituting the values of $\lambda(s_0, e_c)$ and s_0 into Equation (11) gives $\lambda(e_0)$. Using $\lambda(e_0)$, $\lambda(s, e_c)$ for any suction s can be calculated from Equation (11) since $\lambda(0)$ is a model parameter. Therefore, Equations (9) and (11) give the deformation of unsaturated compacted soils with different initial densities and suctions under isotropic compression. The modelling of unsaturated compacted soil behaviour under isotropic compression states takes into account the effects of the initial density on not only the initial yield stress $p'_{y0}(s_0)$, but also the slope $\lambda(s, e_c)$ of the normal compression lines.

As shown in Figure 5, the initial yield stress curve expressed by Equation (7) is assumed to pass through point N, and the co-ordinates of point N (p'_n, e_n) should satisfy Equation (7). Hence, the parameter c in Equation (7) can be calculated from

$$c = \frac{\ln p'_n - \ln b}{\ln e_n} \tag{12}$$

The so-called 'loading-collapse' (LC) yield curve [1] for unsaturated soils with different initial densities is expressed by

$$p'_y = p'_n \left(\frac{p^*_y}{p'_n}\right)^{(\lambda(0)-\kappa)/(\lambda(s,e_c)-\kappa)} \tag{13}$$

where p^*_y is an isotropic yield stress on the normal compression line for a saturated soil and κ is the swelling index of a compacted soil and is assumed to be the same for different initial densities and suctions.

For a given initial density, the initial LC yield curve CDEF and the subsequent LC yield curve GHIJ in Figure 6 are defined using Equations (11) and (13), together with the values of the model parameters and the initial state for compacted Pearl clay (which are given later). When the stress state (p', s) is on the left side of CDEF, there is only elastic deformation occurring during the stress change.

The relationships between dp'_y, dp^*_y and ds, which can be obtained by differentiating Equation (13), are as follows:

$$dp'_y = \frac{\partial p'_y}{\partial p^*_y} dp^*_y + \frac{\partial p'_y}{\partial s} ds \tag{14}$$

DOI: 10.1002/nag

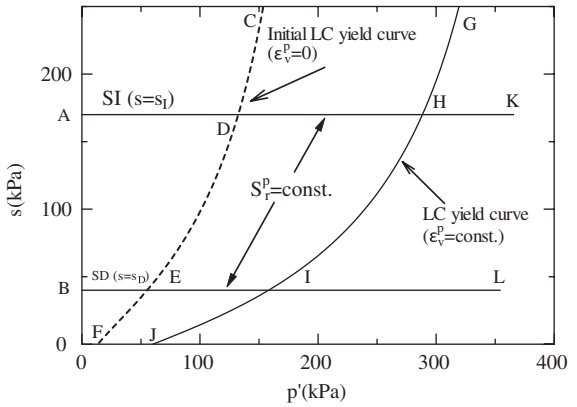

Figure 6. LC yield curve, SI and SD yield curves for compacted Pearl clay under isotropic stress states.

where

$$\frac{\partial p'_y}{\partial p^*_y} = \frac{\lambda(0)-\kappa}{\lambda(s,e_c)-\kappa}\left(\frac{p^*_y}{p'_n}\right)^{(\lambda(0)-\lambda(s,e_c))/(\lambda(s,e_c)-\kappa)} \tag{15}$$

$$\frac{\partial p'_y}{\partial s} == \frac{\lambda(e_0)p_a p'_y(\lambda(0)-\kappa)}{(\lambda(s,e_c)-\kappa)^2(p_a+s)^2}\ln\left(\frac{p'_n}{p^*_y}\right) \tag{16}$$

When the stress state is inside the LC yield curve, the elastic volumetric strain increment is given by

$$d\varepsilon^e_v = \frac{\kappa\, dp'}{(1+e)p'} \tag{17}$$

When the stress state is on the LC yield curve and its increment vector points to the right side of the LC yield curve, the plastic volumetric strain increment is given by

$$d\varepsilon^p_v = \frac{(\lambda(0)-\kappa)\, dp^*_y}{(1+e)p^*_y} \tag{18}$$

Or, from Equation (14)

$$d\varepsilon^p_v = \frac{\dfrac{\lambda(0)-\kappa}{(1+e)p^*_y}\left(dp'_y - \dfrac{\partial p'_y}{\partial s}ds\right)}{\dfrac{\partial p'_y}{\partial p^*_y}} \tag{19}$$

In addition to the LC yield curve, two more yield curves are needed to model hydraulic behaviour as an elastoplastic process, as shown in Figure 6. The water-retention behaviour indicated by Equations (2) and (3) is represented by a SI yield curve and a suction decrease (SD) yield curve in the p'–s plane.

The change in the degree of saturation due to the change in void ratio is attributed to the elastic part of the increment of the degree of saturation. When the change in the degree of

DOI: 10.1002/nag

saturation is elastic, i.e. along the scanning curves, the elastic increment of the degree of saturation can be derived from Equation (1) as follows:

$$\mathrm{d}S_{\mathrm{r}}^{\mathrm{e}} = -\lambda_{\mathrm{se}}\,\mathrm{d}e - k_{\mathrm{s}}\frac{\mathrm{d}s}{s} \tag{20}$$

The plastic change in the degree of saturation can be deduced from Equations (2) and (3) as

$$\mathrm{d}S_{\mathrm{r}}^{\mathrm{p}} = \mathrm{d}S - \mathrm{d}S_{\mathrm{r}}^{\mathrm{e}} = (\lambda_{\mathrm{D}} - k_{\mathrm{s}})\frac{\mathrm{d}s}{s} \quad \text{(for SI)} \tag{21}$$

$$\mathrm{d}S_{\mathrm{r}}^{\mathrm{p}} = \mathrm{d}S - \mathrm{d}S_{\mathrm{r}}^{\mathrm{e}} = (\lambda_{\mathrm{W}} - k_{\mathrm{s}})\frac{\mathrm{d}s}{s} \quad \text{(for SD)} \tag{22}$$

From the condition $\mathrm{d}S_{\mathrm{r}}^{\mathrm{p}} = 0$ we can obtain the following SI and SD yield curves as

$$f_{\mathrm{SI}} = \ln(s_{\mathrm{I}}) + c_1 \quad \text{(for SI)} \tag{23}$$

$$f_{\mathrm{SD}} = \ln(s_{\mathrm{D}}) + c_2 \quad \text{(for SD)} \tag{24}$$

where c_1 and c_2 are integration constants.

For a given plastic change in S_{r}, the SI and SD curves can be drawn as shown in Figure 6. The SI curve AK stems from Equation (23), while the SD curve BL follows from Equation (24). The plastic volumetric strain $\varepsilon_{\mathrm{v}}^{\mathrm{p}}$ is equivalent along the same LC yield curve, with the plastic change in S_{r} being equivalent along the same SI curve or the same SD curve. Therefore, as shown in Figure 6, there are six zones with different yielding characteristics for $\varepsilon_{\mathrm{v}}^{\mathrm{p}}$ and $\mathrm{d}S_{\mathrm{r}}^{\mathrm{p}}$.

(1) When the current stress state (p', s) is on ADH and its increment vector points to the zone ADHG, there is only a plastic change in S_{r} which is given by Equation (21).
(2) When the current stress state (p', s) is on ADH or BEI or HI and its increment vector points to the zone ABEIHDA, there is no change in $\varepsilon_{\mathrm{v}}^{\mathrm{p}}$ and no plastic change in S_{r}.
(3) When the current stress state (p', s) is on BEI and its increment vector points to the zone BEIJ, there is only a plastic change in S_{r} which is given by Equation (22).
(4) When the current stress state (p', s) is on HI and its increment vector points to the zone KHIL, there is only a change in $\varepsilon_{\mathrm{v}}^{\mathrm{p}}$ which is given by Equation (18).
(5) When the current stress state (p', s) is on H and its increment vector points to the zone GHK, there is a change in $\varepsilon_{\mathrm{v}}^{\mathrm{p}}$ and a plastic change in S_{r}. These changes are calculated using Equations (18) and (21), respectively.
(6) When the current stress state (p', s) is on I and its increment vector points to the zone JIL, there is a change in $\varepsilon_{\mathrm{v}}^{\mathrm{p}}$ and a plastic change in S_{r}. These changes are calculated using Equations (18) and (22), respectively.

Figure 7 shows the initial LC yield curves and the initial SI and SD yield curves for an unsaturated soil compacted at different initial densities which are given by Equations (13), (23) and (24). The model predicts that dense compacted specimens have larger initial yield stresses, and higher initial SI and SD yield suctions, as shown in Figures 3 and 1(b), respectively.

3.3. Formulation of the elastoplastic model under general stress states

The modified Cam-clay model has been used extensively for saturated soils and gives reasonably good predictions for clays. This model is adopted here for its simplicity. Experiments under

DOI: 10.1002/nag

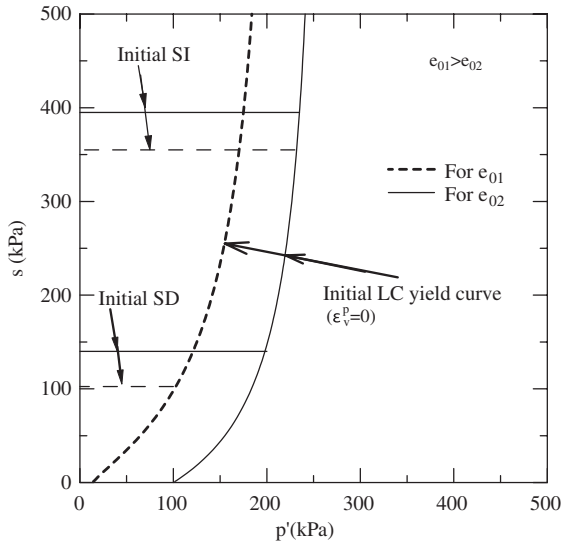

Figure 7. Initial LC yield curves, initial SI and SD yield curves from different initial densities.

general stress states have shown that the Matsuoka–Nakai criterion (also called the SMP criterion, [20]) is applicable to unsaturated soils provided a so-called translated stress is used instead of the traditional effective stress [21]. Here we assume that the SMP criterion is applicable to unsaturated soils using the 'effective stress' under general stress states, and the yield function (f) and the plastic potential function (g) are proposed to have the following form:

$$f = g = \tilde{q}^2 + M^2\tilde{p}(\tilde{p} - p'_y) = 0 \tag{25}$$

where $\tilde{p}$ and $\tilde{q}$ are the invariants of the transformed stress tensor and are defined as [4, 21]

$$\tilde{p} = \tilde{\sigma}_{ii}/3$$

$$\tilde{q} = \sqrt{3(\tilde{\sigma}_{ij} - \tilde{p}\delta_{ij})(\tilde{\sigma}_{ij} - \tilde{p}\delta_{ij})/2} \tag{26}$$

The transformed stress $\tilde{\sigma}_{ij}$ is determined by a transformation of the SMP (solid) curve in the π-plane of the σ'_{ij}-space to a circle (dotted curve) in the transformed π-plane ($\tilde{\pi}$-plane) as shown in Figure 8. Therefore,

$$\tilde{\sigma}_{ij} = p'\delta_{ij} + \frac{\ell_0}{\ell_\theta}(\sigma'_{ij} - p'\delta_{ij}) = p'\delta_{ij} + \frac{\ell_0(\sigma'_{ij} - p'\delta_{ij})}{\sqrt{(\sigma'_{ij} - p'\delta_{ij})(\sigma'_{ij} - p'\delta_{ij})}} \tag{27}$$

where

$$\ell_0 = \frac{2\sqrt{6}I'_1}{3\sqrt{(I'_1I'_2 - I'_3)/(I'_1I'_3 - 9I'_3)} - 1} \tag{28}$$

DOI: 10.1002/nag

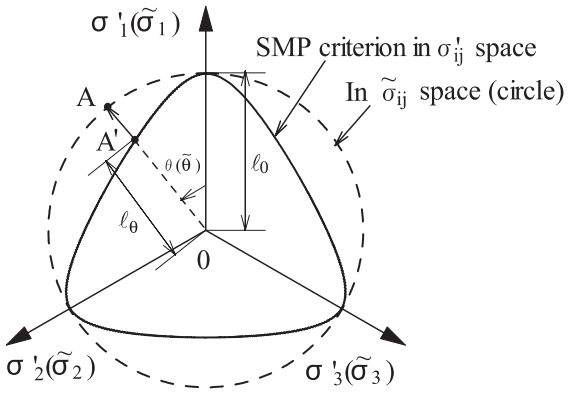

Figure 8. The SMP criterion in the deviatoric planes of 'effective stress' space and transformed stress space.

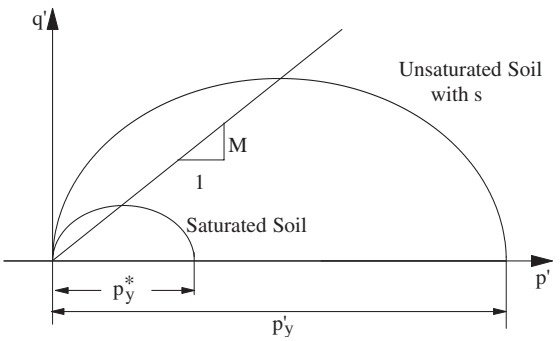

Figure 9. Yield curves under constant suctions.

and I_1', I_2' and I_3' are the invariants of the 'effective stress' tensor σ_{ij}'. Equation (28) is derived from the SMP criterion $I_1' I_2' = (8 \tan^2 \phi_{\text{mob}} + 9) I_3'$ with ϕ_{mob} being the mobilized friction angle [22]. In Equation (25), $\tilde{\sigma}_{ij}$ is used to replace σ_{ij}' when extending the modified Cam-clay model to a three-dimensional elastoplastic model for unsaturated soils. This modification means that the SMP criterion in the 'effective stress' space is introduced to account for the Lode angle dependency of the yield and failure criteria.

Figure 9 shows the geometrical shape of the yield function for $s > 0$ (unsaturated state) and $s = 0$ (saturated state).

A non-associated flow rule is assumed in terms of the 'effective' stresses. In terms of the transformed stresses, however, the flow rule is associated and may be written as

$$\mathrm{d}\varepsilon_{ij}^{\mathrm{p}} = \Lambda \frac{\partial f}{\partial \tilde{\sigma}_{ij}} \tag{29}$$

DOI: 10.1002/nag

where the proportionality constant Λ can be determined from the consistency condition. Rewriting Equation (25) as $f = f(\tilde{p}, \tilde{q}, p'_y) = f(\sigma'_{ij}, p'_y) = 0$ leads to

$$\mathrm{d}f = \frac{\partial f}{\partial \sigma'_{ij}} \mathrm{d}\sigma'_{ij} + \frac{\partial f}{\partial p'_y} \mathrm{d}p'_y = 0 \tag{30}$$

Substituting Equation (14) into Equation (30) and re-arranging gives

$$\mathrm{d}f = \frac{\partial f}{\partial \sigma'_{ij}} \mathrm{d}\sigma'_{ij} + \frac{\partial f}{\partial p'_y} \frac{\partial p'_y}{\partial p^*_y} \mathrm{d}p^*_y + \frac{\partial f}{\partial p'_y} \frac{\partial p'_y}{\partial s} \mathrm{d}s \tag{31}$$

where the isotropic yielding stress p^*_y for saturated soil is related to the plastic volumetric strain ε^p_v and is the same as that used in the traditional Cam-clay model. Because the plastic volumetric strain ε^p_v is one of the hardening parameters in the present model, the plastic volumetric strain increment $\mathrm{d}\varepsilon^p_v$ caused by $\mathrm{d}p^*_y$ in a saturated soil is the same as that in an unsaturated soil which is caused by $\mathrm{d}p'_y$ and/or $\mathrm{d}s$. Substituting Equation (29) into Equation (18), we obtain

$$\mathrm{d}p^*_y = \frac{1+e}{\lambda(0)-\kappa} p^*_y \, \mathrm{d}\varepsilon^p_v = \frac{1+e}{\lambda(0)-\kappa} p^*_y \Lambda \frac{\partial f}{\partial \tilde{p}} \tag{32}$$

Inserting Equation (32) into Equation (31) and solving for Λ gives

$$\Lambda = -\frac{\dfrac{\partial f}{\partial \sigma'_{ij}} \mathrm{d}\sigma'_{ij} + \dfrac{\partial f}{\partial p'_y} \dfrac{\partial p'_y}{\partial s} \mathrm{d}s}{\dfrac{\partial f}{\partial p'_y} \dfrac{\partial p'_y}{\partial p^*_y} p^*_y \dfrac{1+e}{\lambda(0)-\kappa} \dfrac{\partial f}{\partial \tilde{p}}} \tag{33}$$

From Equations (29) and (33), it is possible to calculate the plastic strain increment caused by an increment in the 'effective stress' and/or a decrement in suction.

Following the formulation used in plasticity, the plastic increment of S_r is written as

$$\mathrm{d}S^p_r = \Lambda_\alpha \frac{\partial f_\alpha}{\partial s}, \quad \alpha = \mathrm{SI}, \ \mathrm{SD} \tag{34}$$

where Λ_α are plastic multipliers and can be solved from the consistency condition $\mathrm{d}f_a = 0$. From Equations (23) and (24), we have

$$\frac{\partial f_{SI}}{\partial s} = \frac{1}{s_I} \tag{35}$$

$$\frac{\partial f_{SD}}{\partial s} = \frac{1}{s_D} \tag{36}$$

Substituting Equations (35) and (36) into Equation (34) and then comparing with Equations (21) and (22) gives

$$\Lambda_{SI} = (\lambda_D - \kappa_s) \, \mathrm{d}s \tag{37}$$

$$\Lambda_{SD} = (\lambda_W - \kappa_s) \, \mathrm{d}s \tag{38}$$

DOI: 10.1002/nag

4. COMPARISON OF MODEL PREDICTIONS WITH EXPERIMENTAL RESULTS

4.1. Model parameters and their determination

Because the proposed constitutive model is formulated within an elastoplastic framework, the strain and the degree of saturation consist of elastic and plastic components. The model requires seven parameters to describe the stress–strain behaviour, i.e. $\lambda(0)$, κ, p'_n, e_n, M, b and ν (Poisson's ratio) and six parameters to describe the water-retention behaviour, i.e. λ_D, S^0_{rD}, λ_W, S^0_{rW}, κ_s, and λ_{se}. These model parameters are determined from the results of isotropic consolidation tests with wetting, drying and loading–unloading–reloading processes, followed by subsequent triaxial compression tests on saturated and unsaturated soil specimens under constant suction and constant p (or constant confining net stress).

In total, two tests are required to determine the model parameters. First, an isotropic compression test is conducted under a constant suction of s_1, but only after the unsaturated compacted specimen is subjected to a varying suction from an initial value s_0 to a larger value of s_1 to determine the main drying curve. Secondly, an unsaturated soil specimen with an initial suction of s_0 is loaded to a small net stress (for example, $p = 50$ kPa), and is then wetted to a saturated state under constant net stress. This wetting test is used to determine the main wetting curve. An isotropic compression test (with a loading–unloading–reloading cycle and a subsequent triaxial compression test) is then conducted on this saturated specimen. From the result of the triaxial test on the saturated specimen, the internal friction angle (ϕ or M) can be determined. From the result of the isotropic compression test on the saturated specimen with a loading–unloading–reloading stress path, $\lambda(0)$ and κ can be deduced. The quantities p'_n and e_n can be found from the co-ordinates of the point where the two isotropic compression lines for the saturated and unsaturated specimens intersect. From the result of the isotropic compression test on the unsaturated specimen with a suction of s_1, $p'_{y0}(s_1)$ and $e_c(s_1)$ can be determined. Substituting $p'_{y0}(s_1)$ and $e_c(s_1)$ into Equation (7), and combining the result with Equation (12) gives the value of the parameter b.

The model parameters λ_D, S^0_{rD}, λ_W, S^0_{rW}, κ_s and λ_{se} define the water-retention curve and can be found as follows. λ_{se} is the slope of the e–S_r line under constant suction, so λ_{se} can be determined by plotting e against S_r for an isotropic compression test on unsaturated soil under a constant suction. Thereafter, λ_W and S^0_{rW} are found from the result of the above-mentioned wetting test and λ_D and S^0_{rD} are determined from the result of the above-mentioned drying test. κ_s is determined from the result of the above-mentioned wetting test or drying test.

The elastic component of the soil skeleton strain is calculated from Hooke's law using the 'effective stress', with Poisson's ratio assumed to be $\frac{1}{3}$. The elastic modulus is calculated in the same way as for the Cam-clay model

$$E = \frac{p'(1+e)}{\kappa} \tag{39}$$

The values of the relevant model parameters used in predicting the stress–strain and water-retention behaviour of Pearl clay are summarized in Table I. The model parameters for predicting the stress–strain behaviour are the same as those used previously by Sun *et al.* [12], while the model parameters for predicting the water-retention behaviour are partly new and partly the same as those of Sun and Sheng [11].

DOI: 10.1002/nag

Table I. Model parameters for Pearl clay.

$\lambda(0)$	κ	p'_n (MPa)	e_n	M	b (kPa)	λ_{se}	λ_D	S^0_{rD} (%)	λ_W	S^0_{rW} (%)	κ_s
0.11	0.03	1.62	0.85	1.15	317	0.35	0.27	87.2	0.16	64.5	0.03

In addition to the above-mentioned model parameters, the initial state values including the initial degree of saturation (S_{r0}), initial void ratio (e_0), initial net stress state (σ_{ij0}), and initial suction (s_0) are needed in the model predictions. Unlike other models for unsaturated soils (e.g. [1]), the initial LC yield curve or the initial yield pressure for a given initial density can be determined from Figure 5 and Equations (11) and (13). As shown in Figure 5, when the initial state (S_{r0}, e_0, σ_{ij0} and s_0) is given, point B is determined and so are the values of $p'_{y0}(s_0)$ and $\lambda(s_0, e_c)$. Substituting the values of $p'_{y0}(s_0)$ and $\lambda(s_0, e_c)$ into Equation (13) gives the value of p'_{y0} (the initial yield pressure at a saturated state) and substituting the values of $\lambda(s_0, e_c)$ and s_0 into Equation (11) gives the value of $\lambda(e_0)$. With the above determined values of p^*_{y0} and $\lambda(e_0)$, the initial LC yield curve can be obtained by Equation (13) using the values of the material parameters $\lambda(0)$, κ and p'_n.

4.2. Model prediction versus experimental results under various stress paths

Details of the Pearl clay properties, specimen preparation, triaxial apparatus, and testing procedure can be found in the previous works of Sun *et al.* [4, 10, 12]. These studies provide information about the stress–strain behaviour of Pearl clay, but do not give details of the measured water-retention behaviour. These are given below together with the model predictions.

The stress paths in the predictions are specified in terms of the net stress ($\sigma_{ij} = \bar{\sigma}_{ij} - u_a\delta_{ij}$) and suction s. Increments in σ'_{ij} are given by differentiating Equation (8) according to

$$d\sigma'_{ij} = d(\bar{\sigma}_{ij} - u_a\delta_{ij}) + (S_r\, ds + s\, dS_r)\delta_{ij} \tag{40}$$

Substituting Equations (4)–(6) into Equation (40) gives

$$d\sigma'_{ij} = d(\bar{\sigma}_{ij} - u_a\delta_{ij}) + ((S_r - \kappa_s)\, ds - \lambda_{se} s\, de)\delta_{ij} \tag{41}$$

$$d\sigma'_{ij} = d(\bar{\sigma}_{ij} - u_a\delta_{ij}) + ((S_r - \lambda_D)\, ds - \lambda_{se} s\, de)\delta_{ij} \tag{42}$$

$$d\sigma'_{ij} = d(\bar{\sigma}_{ij} - u_a\delta_{ij}) + ((S_r - \lambda_W)\, ds - \lambda_{se} s\, de)\delta_{ij} \tag{43}$$

Because Equations (41)–(43) involve de, these must to be solved simultaneously with a constitutive model equation before the stress path can be defined in terms of the stress-state variables (the 'effective stress' tensor σ'_{ij} and the suction s).

Figure 10 compares the predicted and measured results for the isotropic compression tests on unsaturated Pearl clay compacted at different initial densities under a constant suction of 147 kPa. This figure shows that the proposed model can predict not only the stress–strain response, but also the change in the degree of saturation for different initial densities under a constant suction of 147 kPa during isotropic loading. The experimental data and predicted results indicate that the degree of saturation increases with increasing mean net stress even under

DOI: 10.1002/nag

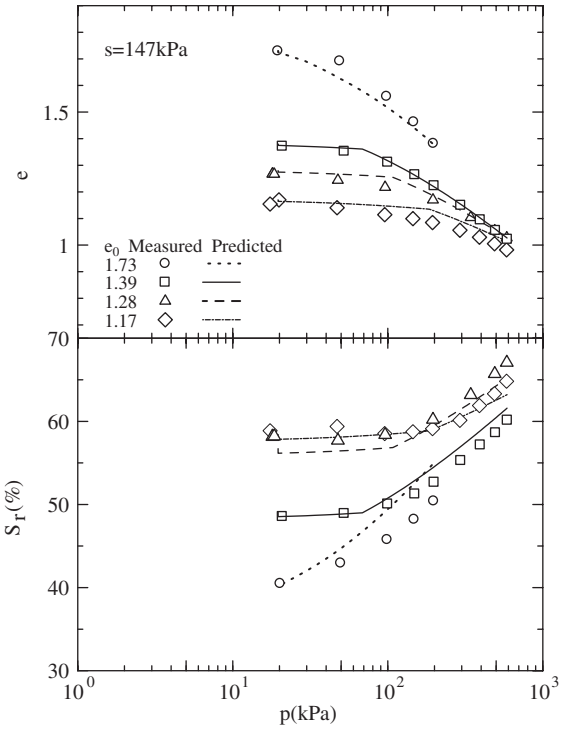

Figure 10. Predicted and measured results of isotropic compression tests on unsaturated Pearl clay with different initial densities under constant suctions.

constant suction. This key feature cannot be predicted by most of the existing constitutive models.

Figure 11 compares the predicted and measured results for the isotropic compression tests under a constant suction of 147 kPa, together with subsequent wetting tests at different isotropic net stresses of 32, 98, 196, 392 and 588 kPa. Y denotes the yielding point at $s = 147$ kPa. The model predicts well the stress–strain response and the water-retention curve during constant suction and also as the suction is decreased from 147 to 0 kPa at different confining stresses. In particular, the model can predict the confining stress dependency of the s–S_r relation (see the lower right-hand figure).

To validate the model performance in predicting the hydraulic and mechanical behaviour under general stress states, triaxial compression tests and triaxial extension tests on unsaturated Pearl clay compacted at different initial densities along the stress paths in Figure 12 were carried out. In this figure, σ_a and σ_r denote the axial and radial stresses in the triaxial tests, respectively. All samples were first subjected to the same stress path ABCC′D and then to different stress paths. C′ denotes the yielding point at $s = 147$ kPa and the position of C′ varies with the initial density.

Figures 13 and 14 compare the predicted and measured results for triaxial compression tests on unsaturated Pearl clay, compacted at different initial densities under constant mean net or effective stress ($p = 196$ kPa), in which a wetting path ($s = 147$ kPa $\rightarrow$ 0 kPa) was imposed at

DOI: 10.1002/nag

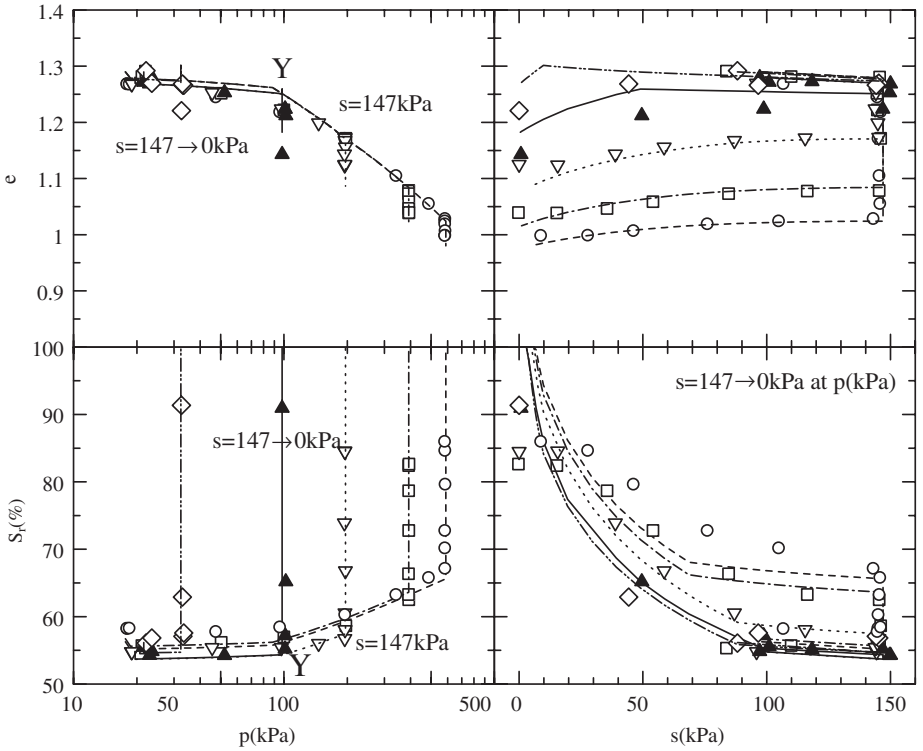

Figure 11. Predicted and measured results of isotropic compression tests for $e_0 = 1.27$.

stress ratios (σ_1/σ_3) of about 1.5 and 2.0, respectively. These figures show that the proposed model predicts the stress–strain and water-retention behaviour of unsaturated compacted clay accurately—not only under constant suction but also under wetting paths in triaxial compression. Note that the model can provide a good prediction of the stress–strain–volume-change behaviour and the water-retention behaviour of unsaturated compacted soil during conditions of constant suction (e.g. D → E in Figure 13 and D → G in Figure 14), suction reduction (E → F in Figure 13 and G → H in Figure 14), and zero suction (F → J in Figure 13 and H → J in Figure 14).

Figures 15 and 16 compare the predicted and measured results for triaxial extension tests on unsaturated Pearl clay, compacted at different initial densities under constant mean net or effective stress ($p = 196$ kPa), in which a wetting path ($s = 147$ kPa → 0 kPa) was imposed at stress ratios (σ_1/σ_3) of about 1.5 and 2.0, respectively. The new model provides good predictions of the stress–strain and water-retention behaviour for different initial densities under constant suction and a wetting path in triaxial extension. This is because the model was constructed for general stress states using three-dimensional yield and failure criteria in σ'_{ij}-space.

From Figures 10 and 11 and 13–16 we may conclude that the proposed model gives good predictions of the stress–strain and water-retention behaviour of unsaturated soil, compacted at different initial densities, during constant suction paths or wetting/drying paths under isotropic or general stress trajectories.

DOI: 10.1002/nag

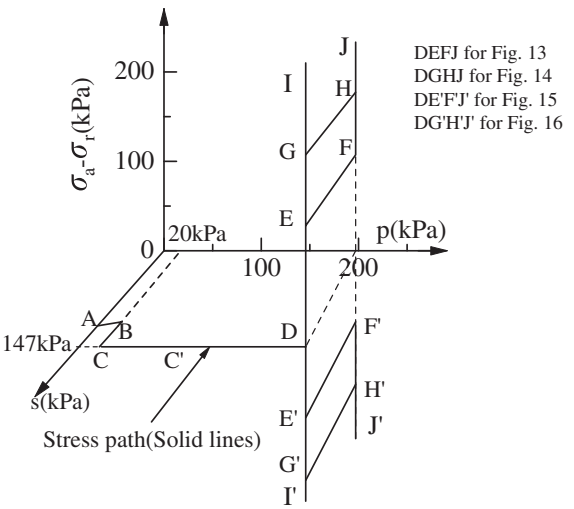

Figure 12. Stress paths for triaxial tests under $p = 196$ kPa.

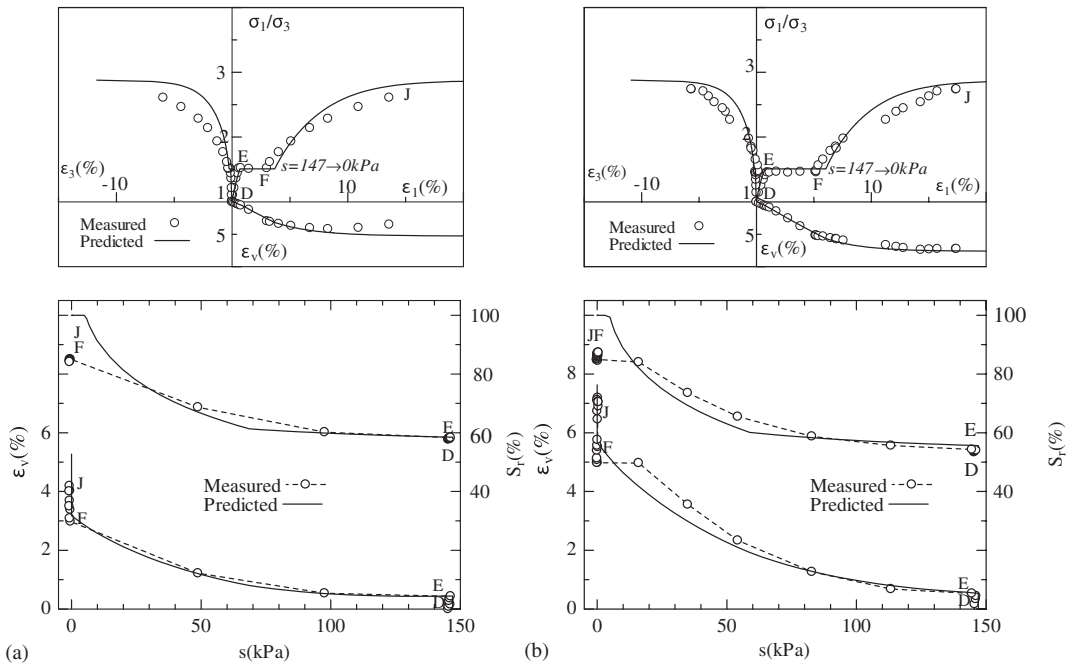

Figure 13. Predicted and measured results for triaxial compression tests on unsaturated compacted Pearl clay at different initial void ratios including wetting at $R = 1.5$ ($p = 196$ kPa): (a) $e_0 = 1.27$; and (b) $e_0 = 1.41$.

DOI: 10.1002/nag

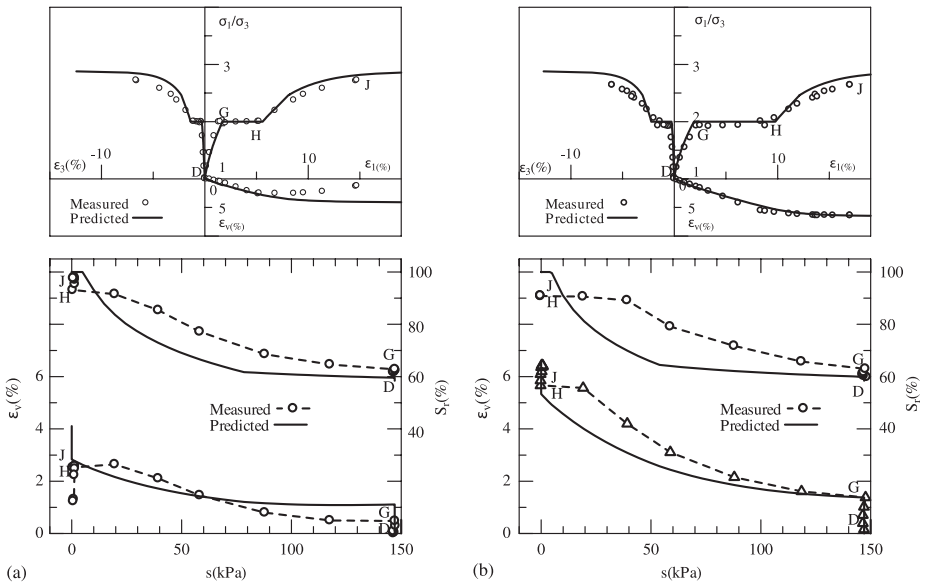

Figure 14. Predicted and measured results for triaxial compression tests on unsaturated compacted Pearl clay at different initial void ratios including wetting at $R = 2.0$ ($p = 196$ kPa): (a) $e_0 = 1.27$; and (b) $e_0 = 1.35$.

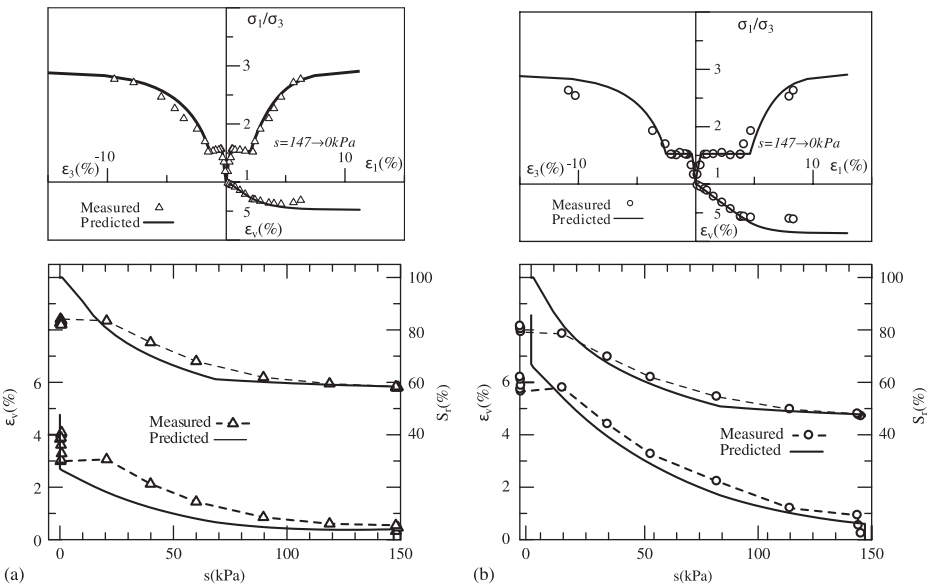

Figure 15. Predicted and measured results for triaxial extension tests on unsaturated compacted Pearl clay at different initial void ratios including wetting at $R = 1.5$ ($p = 196$ kPa): (a) $e_0 = 1.25$; and (b) $e_0 = 1.51$.

DOI: 10.1002/nag

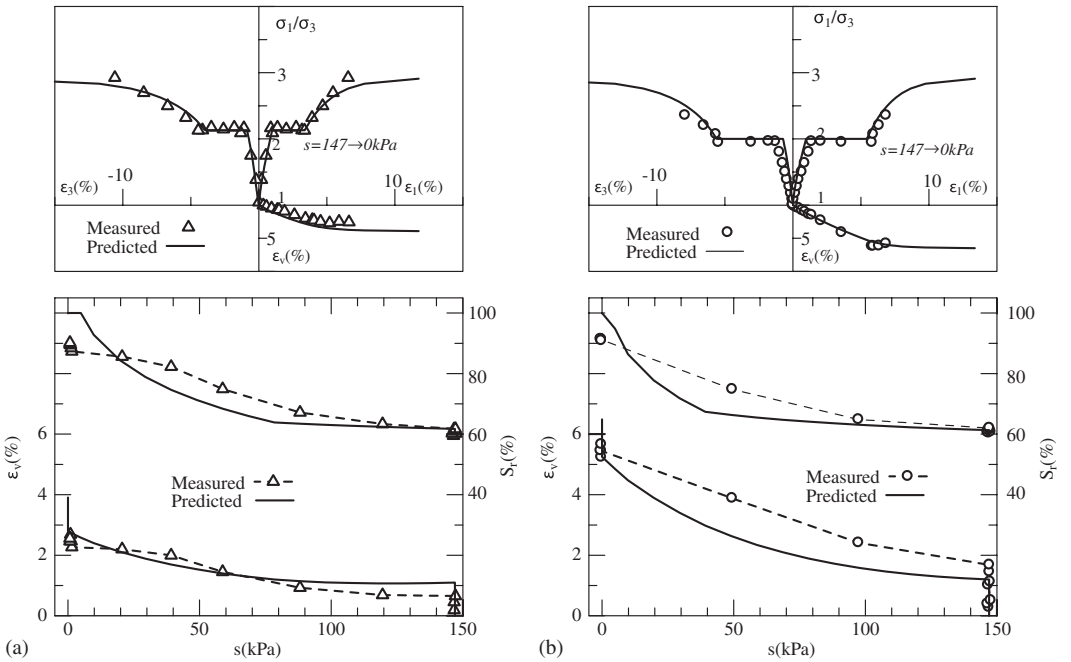

Figure 16. Predicted and measured results for triaxial extension tests on unsaturated compacted Pearl clay at different initial void ratios including wetting at $R = 2.0$ ($p = 196$ kPa): $e_0 = 1.21$; and (b) $e_0 = 1.38$.

5. CONCLUSIONS

(1) The effect of the initial density on the water-retention curve and stress–strain relations were investigated by performing a series of suction-controlled triaxial tests on unsaturated specimens compacted at different initial densities. The test results indicate that the initial density has a major influence on both of these characteristics.

(2) A three-dimensional elastoplastic constitutive model for unsaturated soils with different initial densities, incorporating water-retention behaviour, was proposed. This uses a defined 'effective stress' and suction as the stress-state variables and the soil skeleton strain and the degree of saturation as the strain-state variables. The model is an extension of a hydro-mechanical one developed previously and introduces an initial yield-stress curve for compacted soil. The effects of the suction, the degree of saturation, and the initial density on the stress–strain response, as well as the effects of the suction, the stress state and the initial density on the water-retention behaviour, are taken into account in the proposed model.

(3) A large number of isotropic compression, triaxial compression and triaxial extension tests were carried out on unsaturated clay, compacted at different initial densities, using a suction-controlled triaxial apparatus. During the tests, the strains and water content were measured under stress path control and suction control. In particular, wetting-induced collapse tests, under isotropic or anisotropic stress states, were performed by reducing the

DOI: 10.1002/nag

imposed suction at constant net stress. These gave information on both the deformation and water-retention characteristics. The experimental data are significant for studying the hydro-mechanical behaviour of unsaturated compacted soils.

(4) The proposed model gives good predictions of the stress–strain-strength response and the water-retention behaviour of unsaturated clay compacted at different initial densities along various paths including constant suction paths, wetting paths, drying paths and general net stress paths. Moreover, the hydro-mechanical behaviour of an unsaturated soil compacted at different densities can be modelled using the same material constants.

(5) The model parameters can be determined from isotropic compression tests and triaxial compression tests on two unsaturated specimens with suction control and measurement of water content.

ACKNOWLEDGEMENTS

The authors wish to acknowledge the support provided by the Australian Research Council Discovery grant DP0344417 and the National Natural Science Foundation of China grant 10572082. The authors also wish to thank the anonymous reviewers for their constructive comments.

REFERENCES

1. Alonso FE, Gens A, Josa A. A constitutive model for partially saturated soils. *Geotechnique* 1990; **40**(3):405–430.
2. Kohgo Y, Nakano M, Miyazaki T. Theoretical aspects of constitutive modelling for unsaturated soils. *Soils and Foundations* 1993; **33**(4):49–63.
3. Wheeler SJ, Sivakumar V. An elasto-plastic critical state framework for unsaturated soil. *Geotechnique* 1995; **45**(1):35–53.
4. Sun DA, Matsuoka H, Yao YP, Ichihara W. An elastoplastic model for unsaturated soil in three-dimensional stresses. *Soils and Foundations* 2000; **40**(3):17–28.
5. Dangla P, Malinsky L, Coussy O. Plasticity and imbibition-drainage curves for unsaturated soils: a unified approach. In *Proceedings of the 6th International Symposium on Numerical Models in Geomechanics*, Pietruszczak S, Pande GN (eds). Balkema: Montreal, 1997; 141–146.
6. Buisson MSR, Wheeler SJ. Inclusion of hydraulic hysteresis in a new elastoplastic framework for unsaturated soils. In *Experimental Evidence and Theoretical Approaches in Unsaturated Soils*, Tarantino A, Mancuso C (eds). Balkema: Trento, 2000; 109–119.
7. Vaunat J, Romero E, Jommi C. An elastoplastic hydro-mechanical model for unsaturated soils. In *Experimental Evidence and Theoretical Approaches in Unsaturated Soils*, Tarantino A, Mancuso C (eds). Balkema: Trento, 2000; 121–138.
8. Gallipoli D, Gens A, Sharma R, Vaunat J. An elastoplastic model for unsaturated soil incorporating the effects of suction and degree of saturation on mechanical behaviour. *Geotechnique* 2003; **53**(1):123–135.
9. Wheeler SJ, Sharma RS, Buisson MSR. Coupling of hydraulic hysteresis and stress–strain behaviour in unsaturated soils. *Geotechnique* 2003; **53**(1):41–54.
10. Sheng DC, Sloan SW, Gens A. A constitutive model for unsaturated soils: thermomechanical and algorithmic aspects. *Computational Mechanics* 2004; **33**:453–465.
11. Sun DA, Sheng DC. An elastoplastic hydro-mechanical model for unsaturated compacted soils. In *Advanced Experimental Unsaturated Soil Mechanics*, Tarantino A, Romero E, Cui YJ (eds). Balkema: Trento, 2005; 249–255.
12. Sun DA, Matsuoka H, Cui HB, Xu XF. Three-dimensional elastoplastic model for unsaturated compacted soils with different initial densities. *International Journal for Numerical and Analytical Methods in Geomechanics* 2003; **27**:1079–1098.
13. Estabragh AR, Javadi AA, Boot JC. Effect of compaction pressure on consolidation behaviour of unsaturated silty soil. *Canadian Geotechnical Journal* 2004; **41**(4):540–550.
14. Sun DA, Matsuoka H, Xu YF. Collapse behavior of compacted clays by suction-controlled triaxial tests. *ASTM Geotechnical Testing Journal* 2004; **27**(4):362–370.

DOI: 10.1002/nag

15. Ng CWW, Pang YW. Influence of stress state on soil–water characteristics and slope stability. *Journal of Geotechnical and Geoenviromental Engineering* (ASCE) 2000; **126**(2):157–166.
16. Bishop AW, Blight GE. Some aspects of effective stress in saturated and partly saturated soils. *Geotechnique* 1963; **13**(3):177–197.
17. Lewis RW, Schrefler BA. *The Finite Element Method in the Deformation and Consolidation of Porous Media*. Wiley: Chichester, 1987.
18. Schrefler BA. The finite element method in soil consolidation (with applications to surface subsidence). *Ph.D. Thesis*, University College of Swansea, C/Ph/76/84, 1984.
19. Houlsby GT. The work input to an unsaturated granular materials. *Geotechnique* 1997; **47**(1):193–196.
20. Matsuoka H, Nakai T. Stress-deformation and strength characteristics of soil under three different principal stresses. *Proceedings of Japan Society of Civil Engineers* 1974; **232**:59–70.
21. Matsuoka H, Sun DA, Kogane A, Fukuzawa N, Ichihara W. Stress–strain behaviour of unsaturated soil in true triaxial tests. *Canadian Geotechnical Journal* 2002; **39**(3):608–619.
22. Matsuoka H, Yao YP, Sun DA. The Cam-clay models revised by the SMP criterion. *Soils and Foundations* 1999; **39**(1):81–95.

DOI: 10.1002/nag